buildings

MDPI

Article

Numerical Simulation Study on the Constitutive Model of Fully-Graded Concrete Based on Statistical Damage Theory

Chenyang Yuan [1,2], Chunlei Li [1], Hao Huang [1,*], Weifeng Bai [2,*] and Yunfei Xie [3]

[1] Key Laboratory of Construction and Safety of Water Engineering of the Ministry of Water Resources, China Institute of Water Resources and Hydropower Research, Beijing 100048, China; yuanchenyang@ncwu.edu.cn (C.Y.); lichl@iwhr.com (C.L.)
[2] School of Water Conservancy, North China University of Water Resources and Electric Power, Zhengzhou 450046, China
[3] School of Architecture, North China University of Water Resources and Electric Power, Zhengzhou 450046, China; xieyunfei@ncwu.edu.cn
* Correspondence: huangh@iwhr.com (H.H.); baiweifeng@ncwu.edu.cn (W.B.)

Abstract: A statistical damage model (SDM) of fully-graded concrete was created using statistical damage theory, based on the mechanical properties of axial tension and axial compression of the material. The SDM considers two damage modes, fracture and yield, and explains the intrinsic connection between the mesoscopic damage evolution mechanism and the macroscopic nonlinear mechanical behavior of fully-graded concrete. The artificial bee colony (ABC) algorithm was used to obtain the optimal parameter combination through an intelligent search of parameters ε_a, ε_h, ε_b and H in the constitutive model by taking the test data as the target value, and the sum of the squares of the differences between the target value and the predicted value as the objective function. The SDM numerical simulation model of fully-graded concrete is proposed by compiling subroutines in FORTRAN by constructing two modules of data model and damage analysis. The numerical results under uniaxial and biaxial forces are in agreement with the experimental results, which verifies the accuracy of the program. The model also analyzes the characteristics of mesoscopic damage evolution and predicts the mechanical properties under triaxial forces. The results show that the proposed numerical simulation model can reflect the salient features for fully-graded concrete under uniaxial, biaxial and triaxial loading conditions, and the evolution law of mesoscopic parameters. Therefore, the proposed model serves as a basis for the refined finite element analysis of hydraulic fully-graded concrete structures and reveals the mesoscopic damage mechanism of concrete under different load environments.

Keywords: fully-graded concrete; statistical damage theory; artificial bee colony (ABC); FORTRAN; numerical simulation

check for updates

Citation: Yuan, C.; Li, C.; Huang, H.; Bai, W.; Xie, Y. Numerical Simulation Study on the Constitutive Model of Fully-Graded Concrete Based on Statistical Damage Theory. *Buildings* **2023**, *13*, 2412. https://doi.org/10.3390/buildings13102412

Academic Editor: Francisco López-Almansa

Received: 22 August 2023
Revised: 17 September 2023
Accepted: 20 September 2023
Published: 22 September 2023

Copyright: © 2023 by the authors. Licensee MDPI, Basel, Switzerland. This article is an open access article distributed under the terms and conditions of the Creative Commons Attribution (CC BY) license (https://creativecommons.org/licenses/by/4.0/).

1. Introduction

Fully-graded concrete is a widely used complex nonhomogeneous material in the construction of water conservancy infrastructure—such as gravity dams and arch dams—which consists of cement, aggregate, water and admixture. Compared to conventional concrete particle size, the aggregate size of fully-graded concrete can be up to 150 mm [1]. Concrete has good compressive properties; however, fully-graded concrete structures in real environments are often under multiaxial stresses. The mechanical properties under multiaxial stresses are different compared to uniaxial mechanical properties. The mechanical properties of fully-graded concrete under multidirectional compression have received attention from scholars, and relevant experimental and theoretical research has been carried out [2–4]. The full curve of concrete stress–strain characterizes the whole process of concrete from the beginning of deformation—gradual damage to the final destruction—which can comprehensively reflect the strength and deformation properties of concrete. The multiaxial

stress–strain constitutive relationship is the basis for the refined numerical analysis of the entire process of concrete structures subjected to external loads [5,6]. Since specimens with large-size aggregates are usually larger in size and have higher requirements for the corresponding testing equipment, there are only a limited number of researchers who can carry out the relevant tests. Adopting numerical simulation methods to study the properties of concrete structure, in combination with the relevant test results, to establish a contact between the mesoscopic damage evolution mechanism and the macro mechanical properties, has become one of the research directions of interest to current scientific workers. Therefore, the study of numerical simulation models that can reflect the multiaxial force state of fully-graded concrete is significant for more effective nonlinear analysis and the structural design of large-scale water conservancy projects.

Concrete is a quasi-brittle material, and a scientific and reasonable constitutive model is the key to numerical simulation. Many researchers have investigated the mechanical properties and mesoscopic damage mechanisms of concrete under complex external loads (static, earthquake, explosion [7–11], etc.) through mechanical property tests, and then established a variety of constitutive models. Evabs and Marathe [12] obtained the complete tension stress–strain curve of the concrete for the first time in 1968. Du et al. [13] proposed a special loading machine to obtain the stress-deformation curve and mechanical parameters of concrete and gave an empirical formula. Zhang et al. [14] found that the damage of the specimens manifested mainly in the form of damage at the interface of the aggregate and the mortar bonding, and investigated the law of change of its mechanical properties with external factors. Wang et al. [2] and Shi et al. [3,4] investigated the stress–strain curves and the variation rules of key parameters of dam concrete under different working conditions through a series of uniaxial, biaxial and triaxial tests, and established the constitutive relationship of concrete without an obvious yield surface by applying internal time theory and damage mechanics. The damage mechanic of concrete, which has been developed in recent decades, provides a feasible way for the study of the constitutive relationship of concrete, the typical characteristics of the mechanical properties of concrete can be clearly expressed through the introduction of damage variables, and the damage constitutive model of elastic-plastic damage, which can describe the non-linear behavior of concrete in a more comprehensive way, has been established [15]. Currently, most constitutive models are derived based on experimental fitting of macroscopic stress–strain relationships, and the empirical damage evolution functions are widely adopted in most material models, in which many empirical parameters without clear physical meanings are required [6]. Furthermore, Krajcinovic [16] stated that "an internal variable inferred from phenomenological evidence and selected to fit a particular stress–strain curve may provide a result that pleases the eye, but seldom contributes to understanding of the processes represented by the fitted curve." Among the studies of localized softening of materials, the cohesive cracking model has been promoted as the most fundamental model and is the criterion for judging the correctness of other models. In the study of concrete fracture behavior, Hillerborg et al. [17] were the first to propose the cohesive cracking model, which was later developed into the coated crack zone model [18], but failed to explain what kind of destructive process the material undergoes between cracks. As a typical nonhomogeneous composite material, the essence of concrete damage is the continuous evolution process of microcracks that sprout, expand and nucleate, which is caused by local mesoscopic tensile strains, and the constitutive nonlinear stress–strain relationship shown is the macroscopic manifestation of the nonhomogeneous mechanical properties of mesoscopic components [5]. In order to analyze the mesoscopic characteristics of concrete more deeply, other scholars have introduced advanced methods such as nuclear magnetic resonance (NMR), scanning electron microscopy (SEM), CT technology and acoustic emission technology [19–23] to the study of concrete material damage. This reveals the mesoscopic characteristics of concrete from the aspects of interface transition zone microstructures, pore distribution characteristics, microcrack densities, etc. However, these microscopic analyses have not been able to respond directly to the concrete damage constitutive model.

Many studies have been conducted that explore the complex mechanisms of concrete behavior through experimental and numerical methods. Many scholars have used numerical simulations based on mesostructure to represent the internal structure of the material to explore the concrete damage mechanism. Bažant et al. [24] proposed a random particle model to study the fracture damage of concrete material. This model discretizes the material into a series of particles with only axial contact forces between the particles, and simulates the cracking problem through the tensile destruction of the units. Schlangen et al. [25] proposed a Lattice model to simulate the concrete fracture, and investigated the mesoscopic cracking mechanism of brittle materials in conjunction with experiments. Xu et al. [26] designed a comprehensive numerical framework to statistically characterize the proportion of interfacial transition zones around non-convex aggregates in fully-graded concrete, which was used to assess the physicomechanical properties of fully-graded concrete. Ma et al. [27] developed a three-phase, fully-graded concrete mesoscopic structure model consisting of anisotropic high-content aggregate, cement paste and its interfacial bond, which can qualitatively simulate and explain the influence of mesoscopic structure properties on the macroscopic mechanical properties of fully-graded concrete. Qin et al. [28] used a method that considers the randomness of aggregate geometry and spatial distribution in real engineering to investigate the mesoscopic fracture behavior of fully-graded concrete. Guo et al. [1] investigated the applicability and rationality of the phase field method in the mesoscopic study of fully-graded concrete under uniaxial tension. Xu et al. [29] developed a mesoscale fracture simulation method for fully-graded concrete. Xu et al. [30] proposed a method for generating three-dimensional mesoscale structures of fully-graded concrete: the hierarchical point-cloud method. These studies have played an important role in deepening the understanding of the cracking and damage mechanisms of brittle materials such as concrete, but it is difficult to perform large-scale structural finite element analysis, due to the large number of elements. For the finite element analysis of hydraulic structures such as dams, the Concrete Damaged Plasticity (CDP) model is often used [31–33], which can reflect the macroscopic mechanical behavior of concrete but cannot reveal the mesoscale evolution law. The mesoscopic SDM was developed from continuum damage mechanics to explore the connection between the mesoscopic mechanism of materials and the macroscopic mechanical behavior. Based on the parallel bar system (PBS) proposed by Krajcinovic and Silva [34], which has been improved by many scholars such as Breysse [35], Kandarpa et al. [36] and Bai et al. [37–42], the mechanical properties of recycled concrete have been investigated under the factors of freeze-thaw, age, and strain rate, and the proposed SDM can effectively reveal the intrinsic connection between the mesoscopic damage evolution mechanism and the macroscopic non-linear constitutive behavior of concrete materials.

Despite the significant research carried out in recent years, the task of nonlinear finite element analysis of fully-graded concrete structures is still quite challenging. The accurate modeling of concrete performances is the key issue to numerical simulation. Parameters of the constitutive relationship obtained by fitting the experimental curves do not have clear physical meanings [6,16]; the analysis results based on NMR, SEM, CT, etc. [19–23] cannot be reflected in the constitutive model; it is difficult to analyze large-scale concrete structures using a microscopic model [24–30] that considers mortar matrix, coarse aggregate and interface transition zone; the SDM, which can reflect the microscopic damage mechanism, is currently mainly used to study uniaxial mechanical performance tests of ordinary concrete. Therefore, it is significant to further extend the statistical damage theory to fully-graded concrete, and apply it to numerical simulations. Related research results will contribute to refined finite element analysis of hydraulic structures, reveal mesoscopic damage mechanism and optimize structure design, etc.

In this paper, based on statistical damage theory, combined with the full stress–strain curve of axial tension and axial compression tests, an SDM of fully-graded concrete was established. The ABC method is used to obtain the optimal parameter combinations by intelligent search of the parameters with the test data as the target value, the mesoscopic

parameters in the SDM as the variables and the sum of the squares of the differences between the predicted values and the target value as the objective function. FORTRAN was used to compile the subroutine, two modules of the data model and damage analysis were constructed, and a numerical simulation model of SDM was proposed for fully-graded concrete was proposed. The accuracy of the model was verified by comparing the numerical results with the experimental results, and the characteristics of the evolution of the mesoscopic damage were also analyzed and the mechanical properties were predicted under triaxial forces.

2. Experimental Study on the Mechanical Properties of Fully-Graded Concrete

2.1. Fully-Graded Concrete Specimens

Full-grade concrete specimens were made and tests were carried out according to the Test Procedure for Hydraulic Concrete (SL/T 352-2020) [43]. Ordinary silicate cement—P.O 42.5—was used with a water–cement ratio of 0.42, and the fully-graded concrete mix proportions are shown in Table 1. The dry absorption of saturated surface of sand, small stone, medium stone, large stone and extra-large stone was 1.37%, 0.85%, 0.66%, 0.56% and 0.38%, respectively. In order to improve the workability of concrete mixtures and mitigate the impact of increased hydration temperature on the water–cement ratio, air entraining agents and superplasticizers are incorporated into the mixtures.

Table 1. The mix proportion of fully-graded concrete (kg/m^3).

Cement	FLY Ash	Sand	Small Stone	Medium Stone	Large Stone	Extra Large Stone
315	230	266	272	273	274	276

The size of the axial tension specimen is Φ450 mm × 1470 mm. The specimen is embedded with eight rebar with 32 mm diameter at each end, and the embedding depth is 300 mm. The length of exposed rebar was 60 mm and the screw was machined to a diameter of 22 mm. The arrangement of strain gauges and high-precision extensometers was used to measure the deformation of the specimen, as shown in Figure 1a,c. The strain gauges were arranged on the four sides of the specimen, which were pasted in the axial direction, and each group consisted of 4 strain gauges with a length of 150 mm and the total measuring distance of 660 mm. Four extensometers were arranged in the vicinity of each group of strain gauges, and a total measuring distance was 660 mm. The size of the axial compression specimen used in this study is 450 mm × 450 mm × 450 mm, and strain gauges were used to measure the deformation, as shown in Figure 1b,d. Three 150 mm-long strain gauges and one laser displacement sensor were arranged vertically on each side, for a total of twelve strain gauges and four laser displacement sensors, where the end constraints were as removed by two layers of plastic film and three layers of butter constraints.

2.2. Test Equipment and Loading

In this test, the 15 MN large-scale MTS material testing machine of the China Institute of Water Resources and Hydropower Research is used, as shown in Figure 2, which can meet the requirements of static and dynamic testing of fully-graded concrete.

In axial tension and compression tests, the main test set-up consists of the following components: (1) the actuator is mounted on a crossbeam with a full travel of ±300 mm, hydraulic lift, hydraulic locking and an emergency switch control button; (2) articulated seat assemblies for static and cyclic tests, connected to the actuator and the base, with a rated force of ±1000 kN, swivel angle of +90° or −30° and a tilt angle of ±8°; (3) a 2.5 MN load sensor is used for load measurement and control, with the measurement range of 10~100%, a measurement error less than ±0.5% of the display value and the value variation less than ±0.1% of the display value; (4) temposonic digital displacement transducer is used for deformation measurement, with a stroke of 500 mm, resolution of 0.003 mm. In addition, there are 1500 lpm shunt, coupled accumulator, double-loop inspection valve, etc.

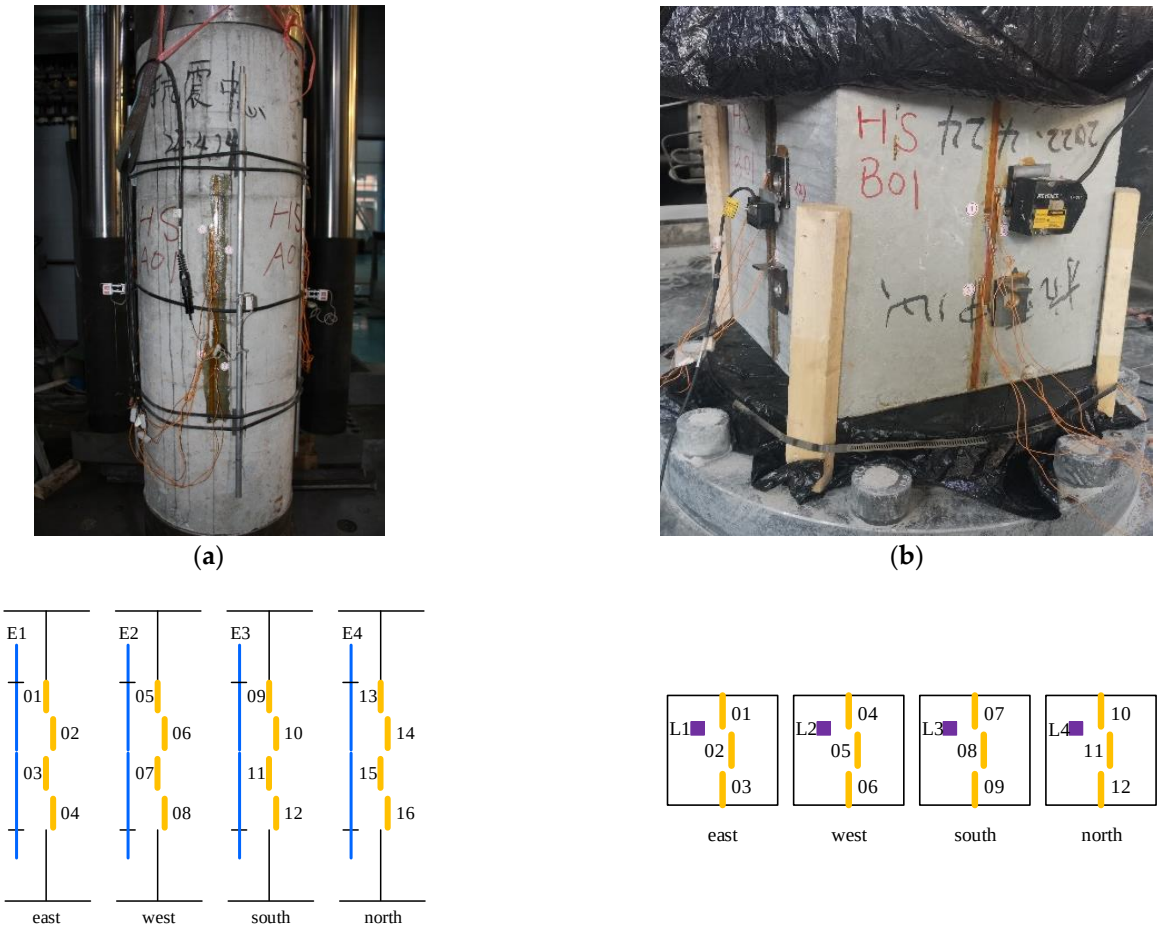


Figure 1. Test specimens: (**a**) axial tension specimen; (**b**) axial compression specimen; (**c**) the arrangement of strain gauges and high-precision extensometers in axial tension specimen; (**d**) the arrangement of strain gauges and laser displacement sensors in axial compression specimen.



Figure 2. The 15 MN large-scale MTS material testing machine.

The MTS FlexTest digital control system is used in this test, which supports a 32 measurement channel return signal control. The system uses a full digital closed-loop control. In order to satisfy different test requirements, the China Institute of Water Re-

sources and Hydropower Research has built a multi-purpose test (MTP) software based on the Level Cross Acquirement function provided by MTS.

For the axial tension test, in order to obtain a complete fully-graded concrete stress–strain curve and capture the damage location, the maximum strain control mode was used in this paper. The maximum value of the 16 strain gauges was used as a control signal to control the loading rate. The schematic diagram of axial tension test is shown in Figure 3. For axial compression test, in order to obtain a complete fully-graded concrete stress–strain curve, the maximum strain control mode was also used in this paper. The maximum value of the 12 strain gauges was used as a control signal to control the loading rate. The schematic diagram of axial compression test is shown in Figure 4.

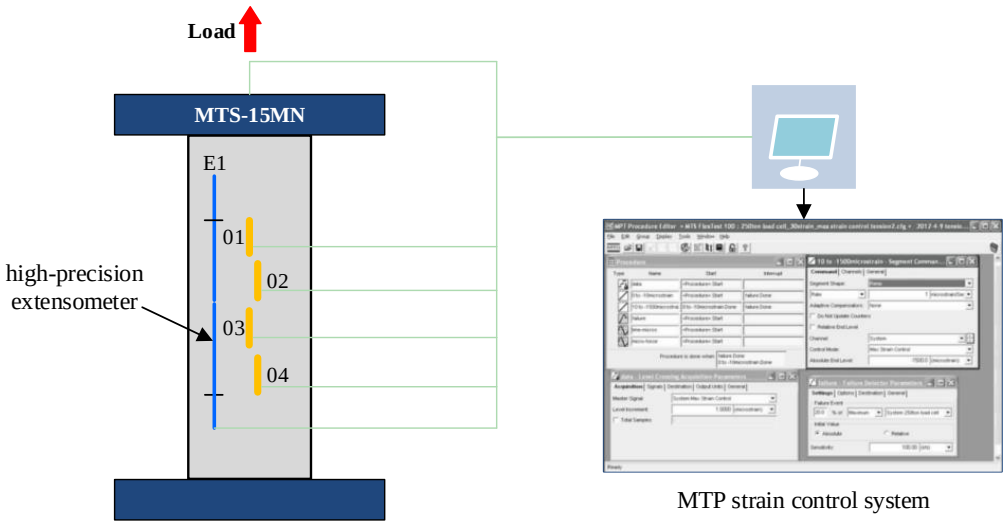


Figure 3. The schematic diagram of axial tension test.

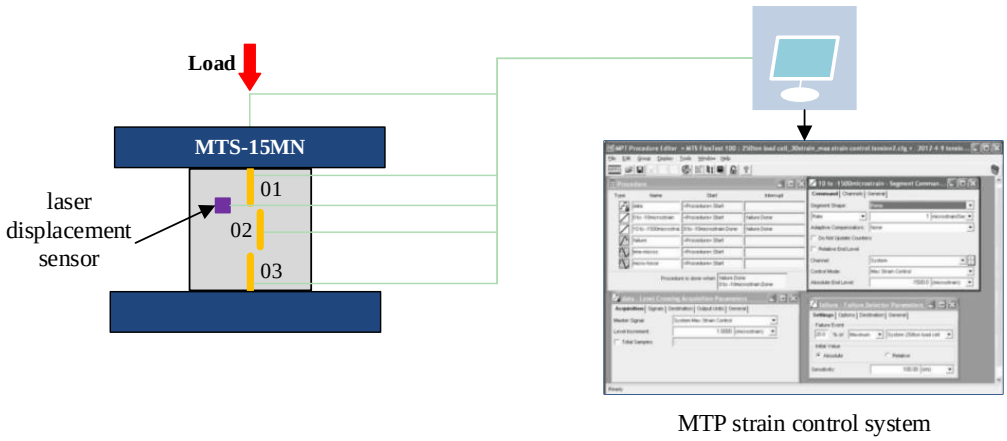


Figure 4. The schematic diagram of axial compression test.

2.3. Test Results

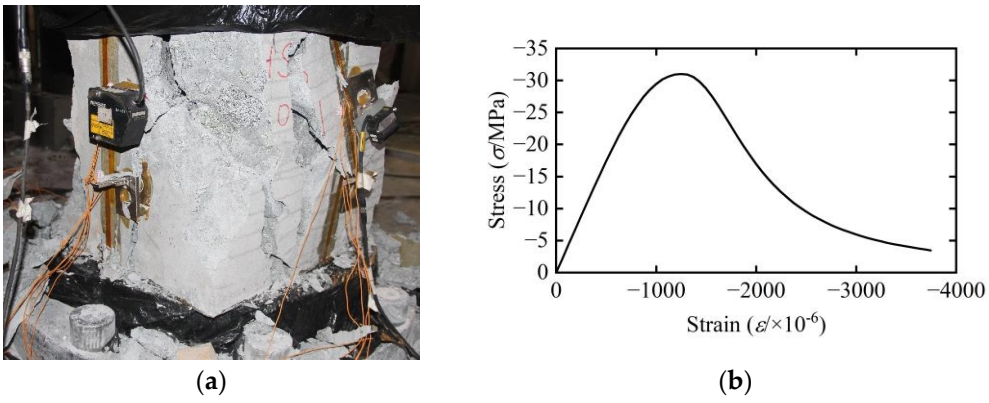
For the axial tension test, with gradual increase in load, the specimen was fractured near its mid-upper position. Figure 5 shows the location of the fracture, typical fracture surfaces and full stress–strain curves. The fracture surface shows damage to the aggregate-mortar bond interface, and the peak strain is 99.87 $\times$ 10^{-6}. The peak stress is 1.73 MPa.

For the axial compression test, the specimen was crushed with a gradual increase of load. The damage state of the compression specimen and the full stress–strain curve are shown in Figure 6. The peak strain is 1248.13 $\times$ 10^{-6} and the peak stress is 31.04 MPa.



(**a**) (**b**) (**c**)

Figure 5. Results of the axial tension test: (**a**) the crack location of tensile damage; (**b**) the section of tensile damage; (**c**) full stress–strain curve.



(**a**) (**b**)

Figure 6. Results of the axial compression test: (**a**) damage under pressure; (**b**) full stress–strain curve.

Through the test results, the macroscopic damage characteristics and the full stress–strain curve of the axial tension and compression tests can be clarified. However, the mesoscopic damage destruction mechanism cannot be revealed.

3. SDM of Fully-Graded Concrete

3.1. Mesoscopic Damage Mechanism and Macroscopic Constitutive Behavior

Bai et al. [5,37–42] proposed a statistical damage theory for concrete, and the concrete is considered a complex system with self-organized behavior. Concrete deformation damage is a process of "adapting" to the external loading environment by further releasing the potential load-bearing capacity through "damage" (microcrack initiation and expansion).

Figure 7 shows the concrete axial tension deformation damage process, which can be divided into two stages of homogeneous damage and localized damage, and contains three typical states: A–C, of which A is the proportional limit state. The direction of stretching is noted as 1-direction, the corresponding nominal and effective stresses are σ_{1A}, σ_{1B}, σ_{1C} and $\sigma_{1E,A}$, $\sigma_{1E,B}$, $\sigma_{1E,C}$, respectively. Due to the non-homogeneity of the mesoscopic composition, the stress state of the internal parts of concrete is different. In the early stage of loading, the load skeleton in the microstructure is not optimized, and some parts with high strength may not even participate in the stressing. With the increase of tensile deformation, a series of

microcracks are randomly generated in weak parts such as aggregate and mortar interfaces, and the direction is roughly perpendicular to the tensile direction. In this process, the weak parts gradually withdraw from the loading, and stress redistribution can be realized. The stronger parts are more involved in the load, and some parts that were not involved in the loading at the beginning are successively added to the load skeleton. By the above method, the effective load skeleton of the microstructure can be further optimized and adjusted, and then the load carrying capacity can be obtained that is consistent with each stress state.

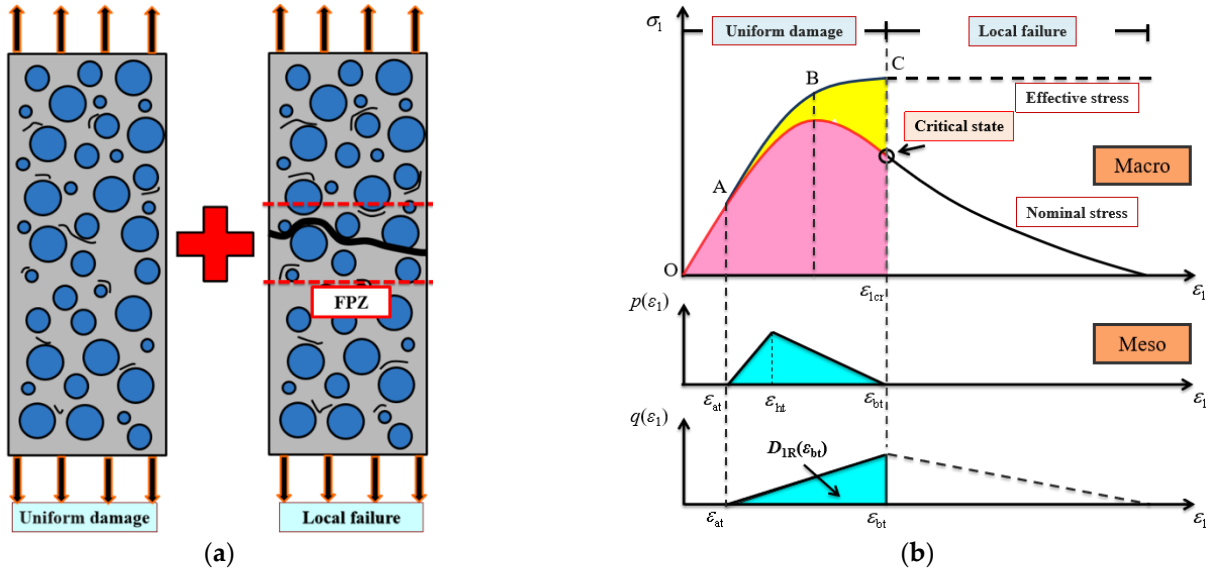


Figure 7. Deformation and failure process of concrete under axial tension: (**a**) two-stage deformation and failure characteristics; (**b**) relationship between mesoscopic damage mechanism and macroscopic nonlinear stress–strain behavior.

Figure 8 shows the damage process of the axial compression deformation of concrete, and the process is also divided into uniform damage and localized destruction of two stages, including the four typical states A–D, of which A is the proportion of the limit state. The direction of compression is noted as the 3-direction, and the two lateral directions as the 1-direction and 2-direction. The nominal and effective stresses corresponding to the compression direction are σ_{3A}, σ_{3B}, σ_{3C}, σ_{3D} and $\sigma_{3E,A}$, $\sigma_{3E,B}$, $\sigma_{3E,C}$, $\sigma_{3E,D}$, respectively. Due to the influence of the Poisson effect, the concrete specimen produces transverse tensile strain in the 1 and 2 lateral directions. When some weak parts of the local tensile strain exceed the ultimate tensile strain, this will lead to the generation of local microcracks. Microcracks first arise and expand at the junction of aggregate and mortar in a direction roughly parallel to the direction of pressure. The microcrack density increases gradually with increasing pressure.

3.2. Statistical Damage Constitutive Model

Bai et al. [5,37–42] established an improved parallel bar system (IPBS) to simulate the axial tensile and compressive deformation and failure processes of concrete, where the compressive direction damage is controlled by the lateral tensile damage process caused by the Poisson effect. In this model, the representative volume element (RVE) in the fracture process zone of material, is assumed as a system composed of T ($T \to \infty$) parallel bars. Each micro-bar is composed of spring, cementation bar and sliding block. Each micro-bar has two feature strains, i.e., the fracture strain and the yield strain, and it may have two kinds of failure modes (fracture and yield). The material disorder is introduced by strain and the yield strain to each bar, which are defined by the independent probability density function $q(\varepsilon)$ and $p(\varepsilon)$, respectively. Therefore, the model considers two damage modes, microscopic fracture and yield, which correspond to the "degradation" and "strengthening" effects of the microstructure, and can be characterized by the fracture and yield of the

microrods, respectively. The mesoscopic inhomogeneity of the material is introduced by assigning random fracture and yield strengths to the microrods. The macroscopic nonlinear stress–strain behavior of concrete is controlled by the evolution of the two damage modes of mesoscopic fracture and yield (in Figures 7b and 8b). The constitutive relationships of axial tensile and compressive statistical damage can be expressed uniformly as follows:

$$\sigma = E_0(1 - D_y)(1 - D_R)\varepsilon \tag{1}$$

$$\sigma_E = E_0(1 - D_y)\varepsilon \tag{2}$$

$$D_y = \int_0^{\varepsilon^+} p(\varepsilon^+)\mathrm{d}\varepsilon^+ - \frac{\int_0^{\varepsilon^+} p(\varepsilon^+)\varepsilon^+\mathrm{d}\varepsilon^+}{\varepsilon^+} \tag{3}$$

$$D_R = \int_0^{\varepsilon^+} q(\varepsilon^+)\mathrm{d}\varepsilon^+ \tag{4}$$

$$E_v = \int_0^{\varepsilon^+} q(\varepsilon^+)\mathrm{d}\varepsilon^+ \tag{5}$$

$$p(\varepsilon^+) = \begin{cases} 0 & (\varepsilon^+ \le \varepsilon_a) \\ \frac{2(\varepsilon^+ - \varepsilon_a)}{(\varepsilon_h - \varepsilon_a)(\varepsilon_b - \varepsilon_a)} & (\varepsilon_a < \varepsilon^+ \le \varepsilon_h) \\ \frac{2(\varepsilon_b - \varepsilon^+)}{(\varepsilon_b - \varepsilon_h)(\varepsilon_b - \varepsilon_a)} & (\varepsilon_h < \varepsilon^+ \le \varepsilon_b) \end{cases} \tag{6}$$

$$q(\varepsilon^+) = \begin{cases} 0 & (\varepsilon^+ \le \varepsilon_a) \\ \frac{2H(\varepsilon^+ - \varepsilon_a)}{(\varepsilon_b - \varepsilon_a)^2} & (\varepsilon_a < \varepsilon^+ \le \varepsilon_b) \end{cases} \tag{7}$$

$$H = D_R(\varepsilon_b) \tag{8}$$

E_v characterizes the degree of optimized adjustment of the microstructure load skeleton and the potential load-bearing capacity. When E_v = 0, it corresponds to the initial state without damage. And when E_v = 1, it corresponds to the critical state with all microbars in the model yield, and the adjustment of the load skeleton is optimized to reach the maximum value. When σ_E reaches its maximum value, the model is about to enter the stage of local destruction. It should be noted that the relevant parameter in the above equation is subscripted as 1 for axial tension, and the relevant parameter in the above equation is subscripted as 3 for axial compression.

The uniaxial SDM of concrete is given above. Considering that concrete will be in two-dimensional or three-dimensional stress state, it is necessary to extend the constitutive model to three-dimensional, which is more conducive to the numerical simulation study.

Based on the assumption of Lamitre equivalent strain, the strain corresponding to the damage state of the material is considered to be equivalent to the ideal elastic state. According to the generalized Hooke's law, the strain components of an elastomer satisfy the following relationship:

$$\varepsilon_i = \varepsilon_{ii} + \varepsilon_{ij} + \varepsilon_{ik}, \quad i, j, k = 1, 2, 3 \text{ and } i \ne j \ne k \tag{9}$$

$$\varepsilon_{ii} = \frac{1}{(1+\nu)(1-2\nu)}\left[(1-\nu)\varepsilon_i + \nu\left(\varepsilon_j + \varepsilon_k\right)\right] \tag{10}$$

$$\varepsilon_{ij} = \frac{\nu}{(1+\nu)(1-2\nu)}\left[(1-\nu)\varepsilon_i + \nu\left(\varepsilon_j + \varepsilon_k\right)\right] \tag{11}$$

Therefore, the three-dimensional damage constitutive equation for concrete can be obtained:

$$\begin{Bmatrix} \sigma_1 \\ \sigma_2 \\ \sigma_3 \end{Bmatrix} = E_0 \begin{bmatrix} (1-D_1) & 0 & 0 \\ 0 & (1-D_2) & 0 \\ 0 & 0 & (-D_3) \end{bmatrix} \begin{Bmatrix} \varepsilon_{11} \\ \varepsilon_{22} \\ \varepsilon_{33} \end{Bmatrix} \tag{12}$$

and

$$D_i = \begin{cases} D_i^+, & \varepsilon_{ii} \geq 0 \\ D_i^-, & \varepsilon_{ii} < 0 \end{cases} \quad i = 1,2,3 \tag{13}$$

According to the assumption of equivalent strain, each strain component in the main direction in the damage state is equivalent to the corresponding strain component in the ideal elastic state, and the following expression can be established as follows.

$$\varepsilon_i^+ = \langle \varepsilon_{ii} + k_1(\varepsilon_{ij} + \varepsilon_{ik}) \rangle (\varepsilon_{ii} \geq 0) \tag{14}$$

where, $\langle\rangle$ is a positive sign, $\langle x \rangle = \begin{cases} x, & x \geq 0 \\ 0, & x < 0 \end{cases}$.

$$k_1 = \begin{cases} k_{10} & \varepsilon_{ij} + \varepsilon_{ik} \geq 0 \\ k_{11} & \varepsilon_{ij} + \varepsilon_{ik} < 0 \end{cases} \tag{15}$$

$$\varepsilon_i^* = \max\{\langle \varepsilon_{ij} + k_2\varepsilon_{ii} + k_3\varepsilon_{ik} \rangle\} \quad (i,j,k = 1,2,3; \ i \neq j \neq k) \tag{16}$$

$$k_2 = \begin{cases} k_{20} & \varepsilon_{ij} \geq 0 \\ k_{21} & \varepsilon_{ii} < 0 \end{cases}; \quad k_3 = \begin{cases} k_{30} & \varepsilon_{ik} \geq 0 \\ k_{31} & \varepsilon_{ik} < 0 \end{cases} \tag{17}$$

$$\varepsilon_i^- = \sqrt{\frac{1}{2}\left[\left(\varepsilon_j^*\right)^2 + \left(\varepsilon_k^*\right)^2 \right]} \quad (i,j,k = 1,2,3; \ i \neq j \neq k) \ (\varepsilon_{ii} < 0) \tag{18}$$

In order to be consistent with the intrinsic direction of uniaxial compression, this function is written in this paper in the form of Equation (18).

It should be noted that axial tensile and compression constitutive models are special cases of the three-dimensional constitutive model.

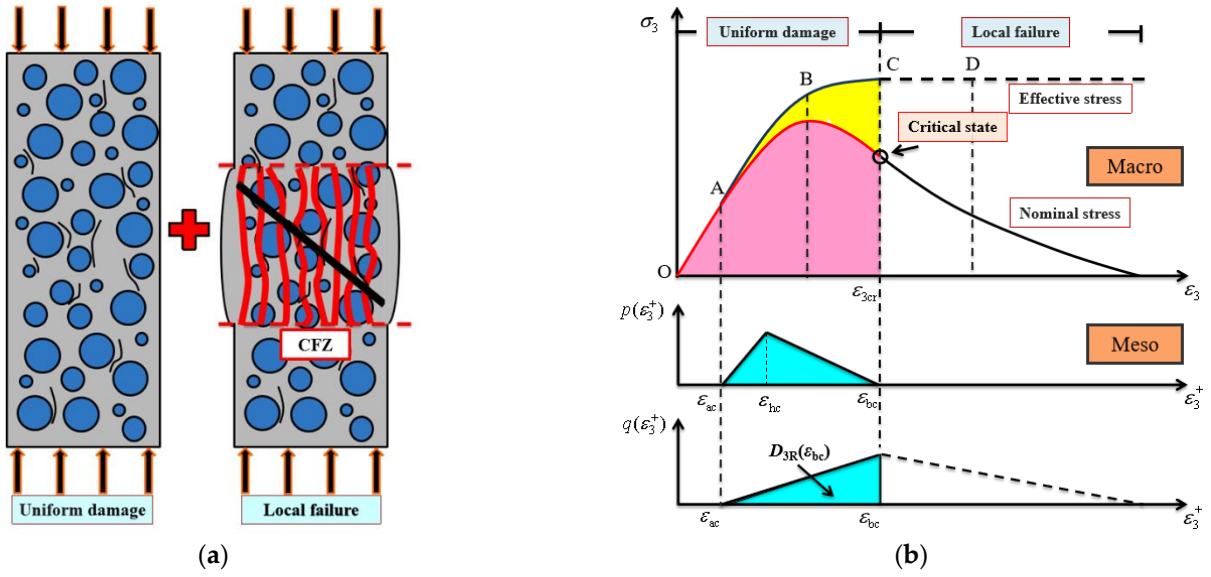


Figure 8. Deformation and failure process of concrete under axial compression: (**a**) two-stage deformation and failure characteristics; (**b**) relationship between mesoscopic damage mechanism and macroscopic nonlinear stress–strain behavior.

3.3. Parameterization Method Based on ABC

SDM can establish an effective link between the mesoscopic damage mechanisms of concrete and the nonlinear macroscopic behavior. The determination of the ε_a, ε_h, ε_b and H parameters is the key to obtaining the constitutive relationship of fully-graded concrete. The ABC method is used to obtain the optimal parameter combinations by intelligent search of the parameters with the test data as the target value, with the mesoscopic parameters ε_a, ε_h, ε_b and H in the SDM as the variables, and the objective function is constructed by solving the sum of the squares of the differences between the target and predicted values corresponding to all data points. Then the SDM of concrete can be obtained (Figure 9).

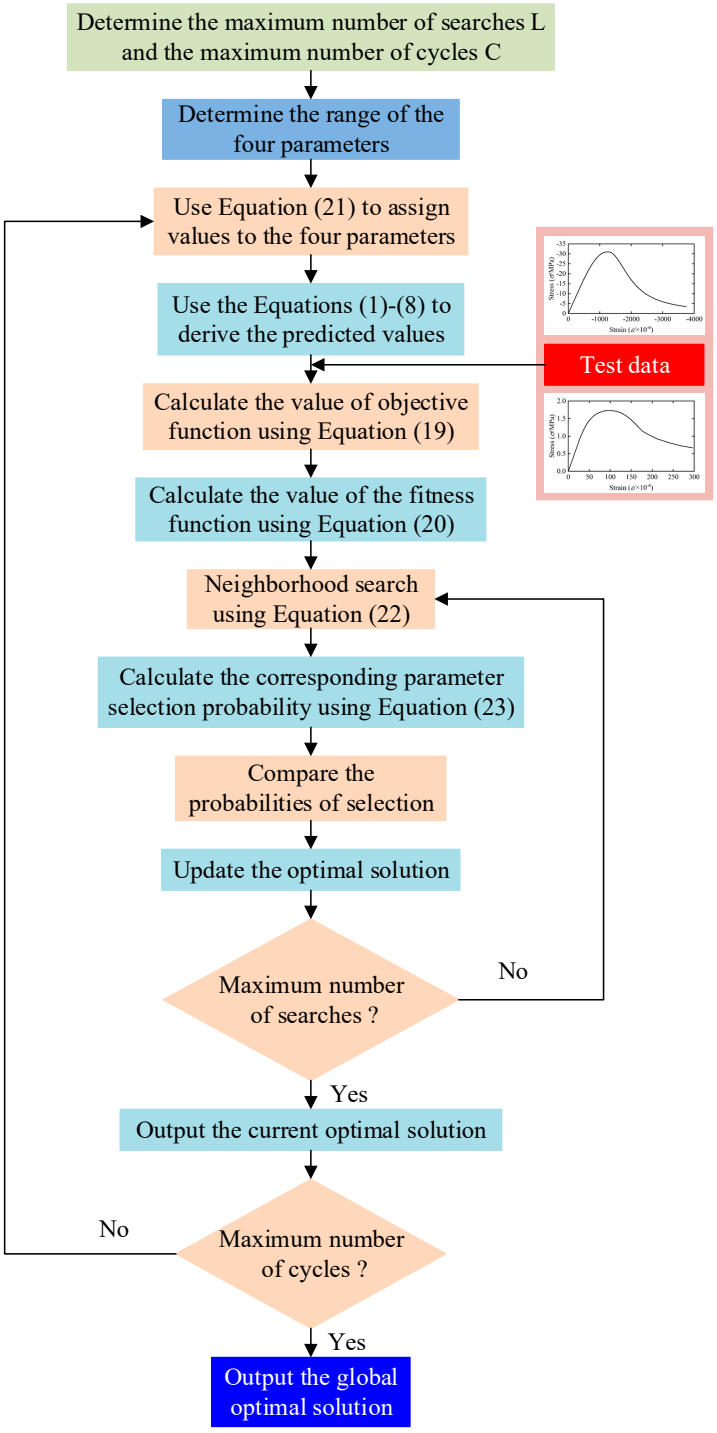


Figure 9. Flowchart for determining parameters of SDM for concrete based on ABC.

The detailed steps are as follows:

① Obtain stress–strain curves from axial tensile or compressive test of fully-graded concrete specimens.

② Establish the objective function. The sum of the squares of the differences between the target and predicted values corresponding to all data points is taken as the objective function, as shown in Equation (19):

$$F = \sum_{n=1}^{N} (x_{tn} - x_{en})^2 \tag{19}$$

where $n = 1, 2, 3, \ldots, N$. The objective is to minimize the objective function. The predicted values are obtained by Equations (1)–(8) under a set of values for ε_a, ε_h, ε_b and H.

③ Determine the fitness function. The ABC algorithm will always choose a larger fitness value when searching, so the inverse of the objective function F is chosen as the fitness function, as shown in Equation (20):

$$f = \frac{1}{\sum_{n=1}^{N} (x_{tn} - x_{en})^2} \tag{20}$$

④ Determine the maximum number of searches L and the maximum number of cycles C.

⑤ Determine the parameter search range. For the four parameters, the ranges of ε_a, ε_h, ε_b and H are given by combining the ontological relationship and experimental data, and each parameter is assigned a value to X_r according to Equation (21):

$$x_{tr} = x_{\min,r} + rand(0,1)(x_{\max,r} - x_{\min,r}) \tag{21}$$

where, $r = 1, 2, 3, 4$, and $X_1 = \varepsilon_a, X_2 = \varepsilon_h, X_3 = \varepsilon_b, X_4 = H$. $rand(0,1)$ is a random number in the range (0, 1).

⑥ Search parameters. For the four parameters, a neighborhood search is performed according to Equation (22):

$$x'_m = x_{tr} + \varphi_{tr}(x_{tr} - x_{sr}) \tag{22}$$

where, $m = 1, 2 \ldots L$, and $t \neq s$.

⑦ Calculate the current optimal solution. Calculate the selection probability according to Equation (23):

$$p = f_z \Big/ \sum_{u=1}^{z} f_u \tag{23}$$

where, $u = 1, 2, 3, \ldots, z$.

Neighborhood search of x_{tr} according to Equation (22) yields the parameter $x_1^{'}$, and the associated fitness $f_1^{'}$ and selection probability $p_1^{'}$ are calculated according to Equations (20) and (23).

If $p_1' > p$, then the current optimal solution is ${x_{tr}}^d = x_1'$. p denotes the selection probability corresponding to x_{tr}.

If $p_1' \leq p$ and the maximum number of searches has not been reached, step ⑦ is repeated to rerun the neighborhood search.

If the maximum number of searches is reached without obtaining a greater probability of selection, then $p_1' \leq p$ is the current optimal solution.

⑧ Calculate the global optimal solution. Calculate the fitness f^d and selection probability p^d corresponding to all current optimal solutions ${x_{tr}}^d$ according to Equations (20) and (23). Compare all selection probabilities p^d and take the current optimal solution ${x_{tr}}^d$ with the largest selection probability p^d as the optimal solution and output $X_r = {x_{tr}}^d$.

According to statistical damage theory, a reasonable range of values for the four parameters needs to be determined. Based on the axial tensile test data of fully-graded concrete, the value ranges of ε_a, ε_h, ε_b and H were selected as [0.0001, 0.2], [0.2001, 1], [1.0001, 3] and [0.0001, 1], respectively. Based on the axial compression test data, the value

ranges of ε_a, ε_h, ε_b and H were selected as [0.0001, 1], [1.0001, 3], [3.0001, 5] and [0.0001, 1], respectively. The maximum number of searches is set at 50 and the maximum number of loops is set at 100, then the parameter optimization is carried out according to the method proposed in Figure 9.

For the axial tension test, the modulus of elasticity is 3.55×10^4 MPa, and the optimal parameters of ε_a, ε_h, ε_b and H are 0.0495, 0.2488, 1.4423 and 0.2663, respectively; for the axial compression test, the modulus of elasticity is 3.55×10^4 MPa, the optimal parameters of ε_a, ε_h, ε_b and H are 0.6548, 2.6848, 3.6711 and 0.4965, respectively. Figures 10 and 11 show the optimization process of axial tensile and compression parameters, and the comparison curves of test and fitting results. It can be seen that the ABC method is able to converge to the optimal result very quickly, and the nominal stress–strain curves predicted by the model are in good agreement with the experimental curves. This validates the effectiveness of the methodology in this article.

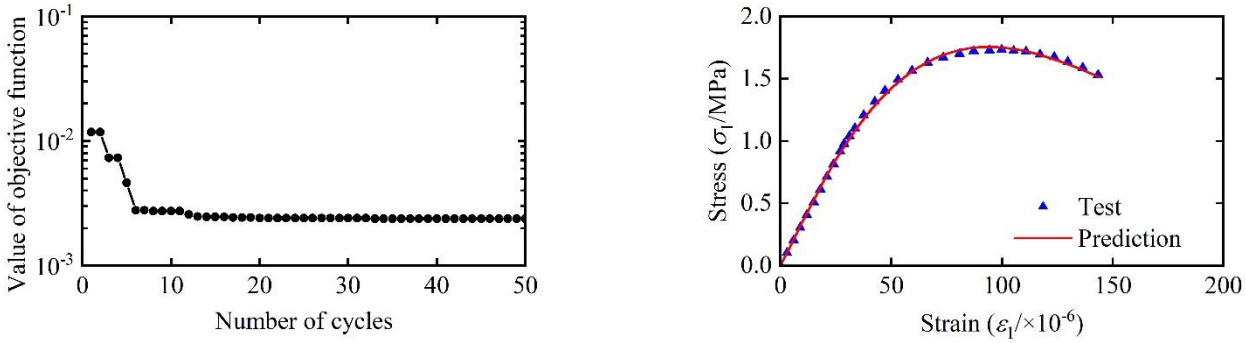


Figure 10. Determination of axial tension parameters: (**a**) number of cycles and objective function; (**b**) comparison of experimental and fitted results.

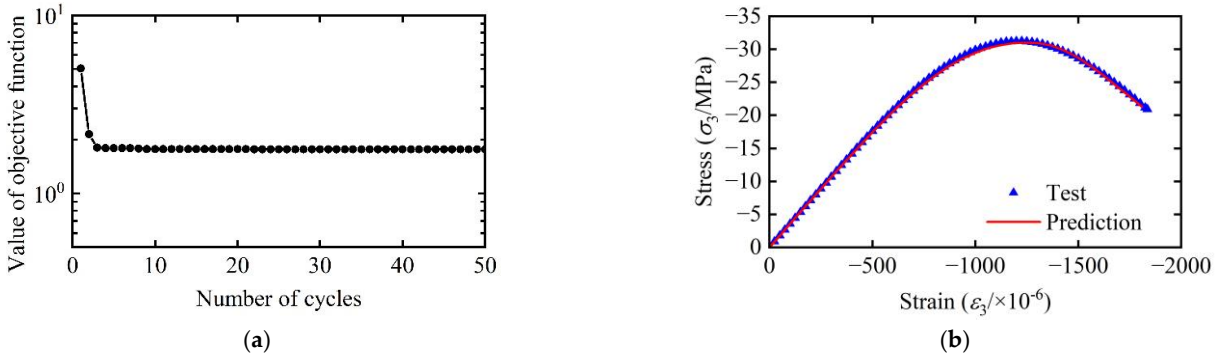


Figure 11. Determination of axial compression parameters: (**a**) number of cycles and objective function; (**b**) comparison of experimental and fitted results.

4. Numerical Implementation of SDM

The SDM developed in this paper is capable of characterizing the mesoscopic fracture and yield damage evolution process of concrete and revealing the relationship between the mesoscopic damage mechanism and the macroscopic nonlinear stress–strain behavior. In order to apply the model to the analysis of fully-graded concrete structures, numerical implementation is necessary.

The numerical implementation process of the model can be divided into two parts: (1) the establishment of the physical model and attribute assignment; (2) the finite element method solution, including the displacement field, stress field, strain field, etc. Then the evolution of the mesoscopic damage of the element is analyzed. Figure 12 shows the numerical analysis process and calculation scheme. The detailed steps are as follows:

① Establish a finite element model;
② Obtain model data for the S-th loading step;
③ Perform the w-th sub-step calculation (w initial value is 0);
④ Solve the finite element equations and update the element elastic strain;
⑤ Update the element stresses;
⑥ Calculate the three principal strains;
⑦ According to the SDM, determine whether the element produces damage or not: if there is damage, calculate the damage value, carry out the stiffness degradation treatment, and repeat step ④; if there is no damage, carry out the next step;
⑧ According to the load applied in sub-step w, determine whether the end of the sub-step: if the end requirements are not met, make $w = w + 1$ and repeat step ③; if the end requirements are met, go to the next step;
⑨ According to the overall load application, judge whether to end the load step: if the end requirements are not met, make $S = S + 1$ and repeat step ②; if the end requirements are met, end the calculation.

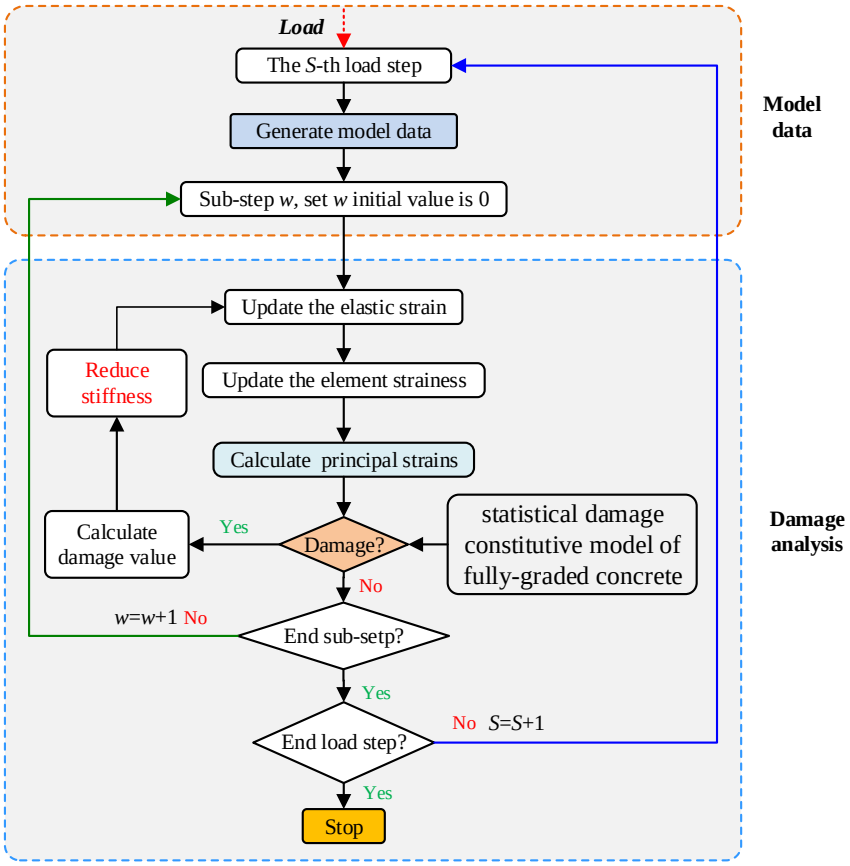


Figure 12. Numerical analysis process and calculation scheme.

In order to meet the requirements of the static method and consistent with the quasi-static damage process of the concrete test, the loading step should be controlled in the quasi-static range. In the loading process, it is important to set the loading step reasonably, because too large a loading step will lead to a large one-step error, and too small a loading step will increase the amount of calculation.

In this paper, the numerical simulation of SDM is realized through FORTRAN programming, and the whole process is to embed the FORTRAN program into the finite element software to analyze the damage evolution characteristics of the structure.

5. Results

Figure 13 gives the overall numerical simulation idea of fully-graded concrete constitutive model. First, the full stress–strain curves are obtained by axial tensile and compression tests, then the SDM of fully-graded concrete is established, the main parameters of the constitutive model are determined based on the ABC algorithm, and finally the FORTRAN subroutine is compiled to realize the numerical simulation calculation. In order to verify the accuracy of the proposed numerical simulation method, a finite element model with a single element is established, as shown in Figure 14a, while Figure 14b shows the boundary conditions. The uniaxial, biaxial, and triaxial forces are analyzed. It should be noted that the compression and tension modulus of elasticity are assumed to be the same, and Poisson ratio is 0.2 during the numerical simulation.

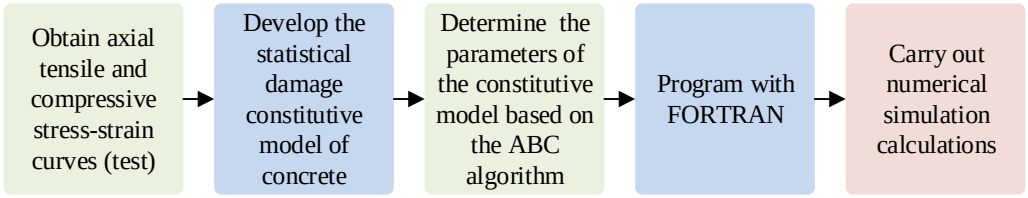


Figure 13. Overall idea of numerical simulation of fully-graded concrete constitutive model based on statistical damage theory.

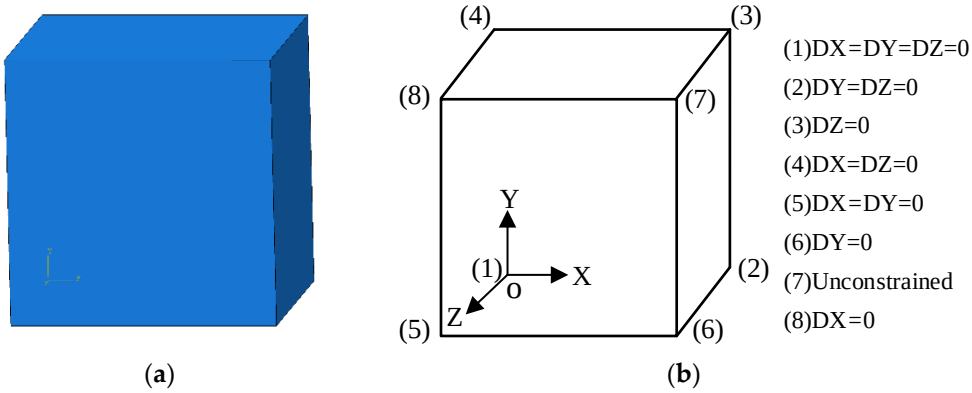


Figure 14. Numerical simulation model: (**a**) finite element model; (**b**) node numbering and boundary conditions.

5.1. Numerical Simulation of Uniaxial Force

Based on the boundary conditions in Figure 14b, the axial tensile case is simulated by applying the positive displacement in the Y-direction, and the axial compression case is simulated by applying the negative displacement in the Y-direction. Comparisons of the axial tension and compression simulation results with the test results are given in Figure 15. It can be seen that the nominal stress–strain full curves of the numerical simulation match well with the test results, which also shows that the proposed simulation method can simulate the uniaxial stress situation well. Figure 16 shows the evolution curves of the fracture damage variables D_{1R} and D_{3R}. For axial tensile, microcracks begin to develop in small strains and gradually expand until the specimen enters a state of destruction. For axial compression, microcracks begin to develop at a strain of 400×10^{-6} and gradually expand, and D_{3R} is 0.47 at a strain ε_3 of 1800×10^{-6}. Figure 17 shows the evolution curves of evolutionary factors E_{1v} and E_{3v}. For axial tension and axial compression, the value of E_v ranges from 0 to 1 and the evolution curve is S-shaped.

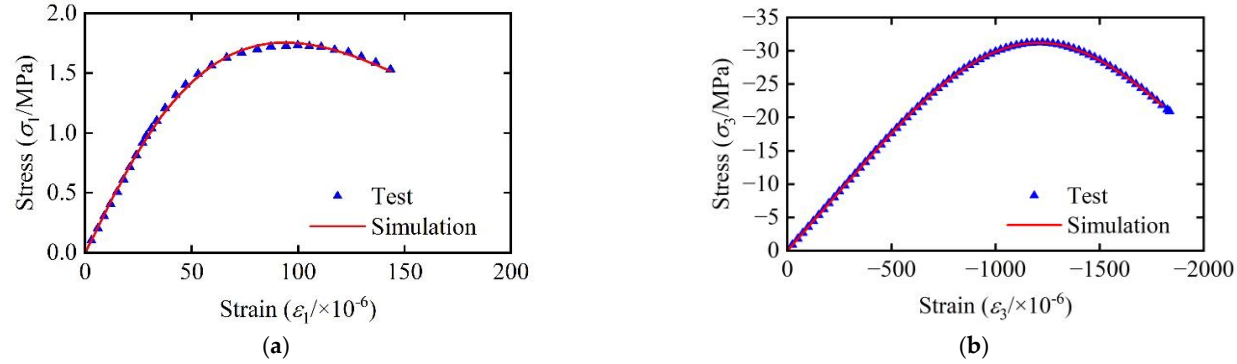


Figure 15. Comparison of the nominal stress–strain curves obtained from numerical simulation and test: (**a**) axial tension; (**b**) axial compression.

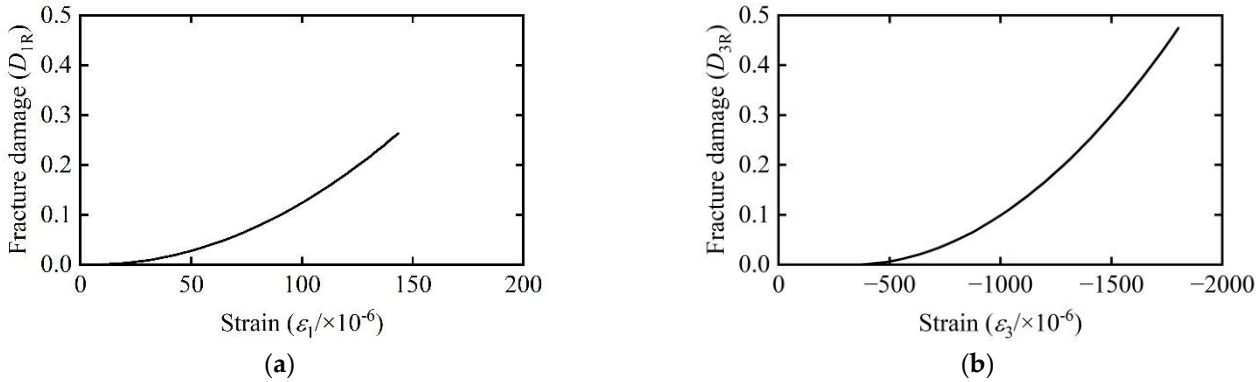


Figure 16. Evolution curves of D_R: (**a**) axial tension; (**b**) axial compression.

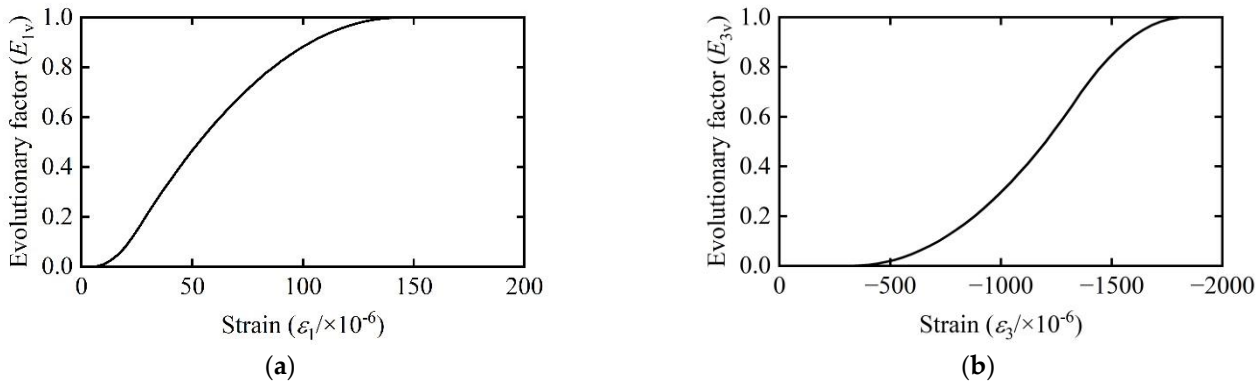


Figure 17. Evolution curves of E_v: (**a**) axial tension; (**b**) axial compression.

5.2. Numerical Simulation of Biaxial Forces

In practice, hydraulic structures are not only under simple uniaxial loads, but also under complex multiaxial loads. Wang et al. [2] investigated the stress characteristics of fully-graded concrete under different stress ratios through experiments. Referring to the relevant data of Wang et al. [2], the mesoscopic parameters of the SDM were determined by the ABC algorithm and then combined with the FORTRAN subroutine to perform the biaxial forces state analysis. Based on the boundary conditions in Figure 14b, the biaxial compression state is realized by applying negative displacement in the Y direction and negative displacement in the X direction, and the analysis is carried out for four working conditions with stress ratios of 0, 0.25, 0.5 and 1. It should be noted that loading is controlled by the strain ratio during the numerical simulation, but Wang et al. [2] controlled the loading by the stress ratio during the experiment. Therefore, the corresponding stress ratio needs to be obtained by trial calculation. For stress ratios α of 0 and 1, the strain ratios

and stress ratios are identical. For the stress ratio of 0.25, the X-direction to Y-direction strain ratio of 0.053 is chosen, and the calculated stress ratio is in the range of [0.2497, 0.2503]; for the stress ratio of 0. 5, the X-direction to Y-direction strain ratio of 0.34 is chosen, and the calculated stress ratio is in the range of [0.4994, 0.5068].

Figure 18 shows the comparison between the simulation results and the test results for the four working conditions. It can be seen that the nominal stress–strain curves calculated by simulation are in good agreement with the test curves. The peak stresses corresponding to the four conditions are 20.67 MPa, 28.51 MPa, 27.83 MPa and 26.57 MPa, respectively. The condition with stress ratio of 0 is an axial compression state. For the other three conditions, the peak stress is found to decrease with an increase in the stress ratio. In order to further clarify the change rule of biaxial forces state, biaxial compression-compression, biaxial tension-compression and biaxial tension-tension and other working conditions are analyzed, the biaxial relative strength envelope in the stress space is plotted, as shown in Figure 19. The evolution curves of D_{3R} and E_{3v} for different stress ratios are shown in Figure 20. For the stress ratio α of 0, the evolution curves are consistent with the characteristics of axial compression.

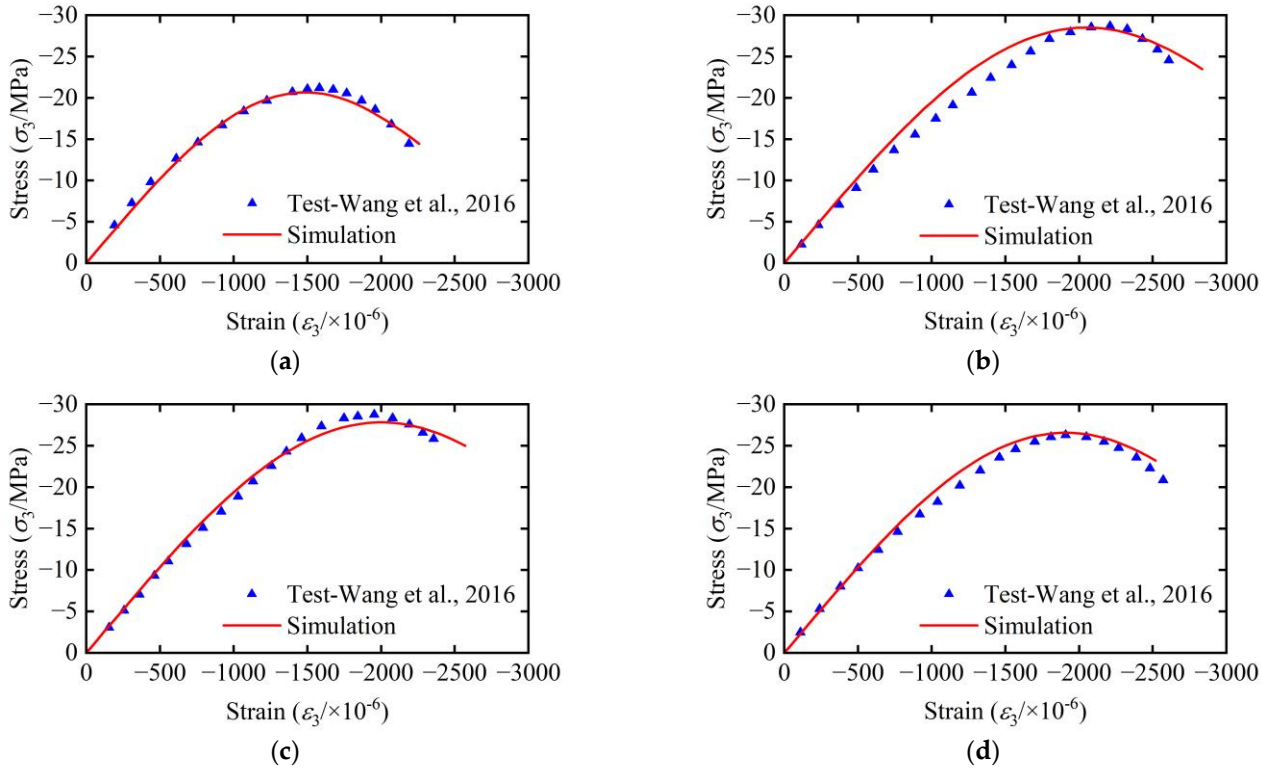


Figure 18. Nominal stress–strain full curve for biaxial compression-compression: (**a**) α = 0; (**b**) α = 0.25; (**c**) α = 0.5; (**d**) α =1 [2].

5.3. Numerical Simulation of Triaxial Forces

The mechanical properties of fully-graded concrete under the state of triaxial forces are complex. There are relatively few valid experimental results in the literature, and the experimental studies are mainly focused on the triaxial compression-compression-compression state. A numerical simulation of the constitutive behavior of fully-graded concrete under triaxial compression-compression-compression condition is carried out using the model of this paper. Strain-controlled proportional loading is used in two modes: $\varepsilon_1 = \varepsilon_2 > \varepsilon_3$ and $\varepsilon_1 > \varepsilon_2 = \varepsilon_3$. For the two modes, six working conditions are analyzed, and the nominal stress–strain curves corresponding to different working conditions are shown in Figure 21. It can be seen that the peak stress and peak strain are different for different strain ratios, which further shows the complexity of the triaxial stress state. The evolution curves of D_{3R} and E_{3v} under different working conditions of the two modes are

given in Figures 22 and 23, respectively, and the change rule of D_{3R} and E_{3v} reveals the mesoscopic mechanism of the macroscopic stress–strain curve.

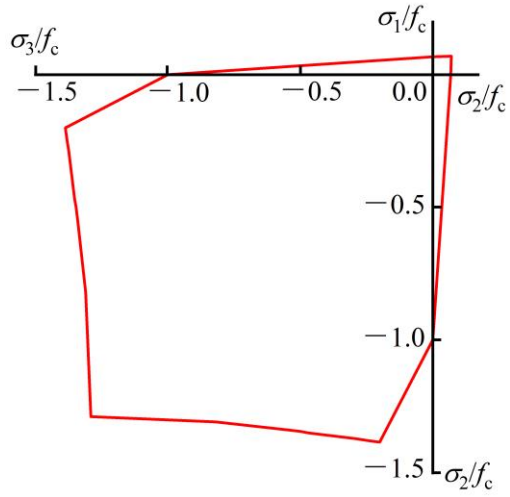


Figure 19. Biaxial relative strength envelope in stress space.

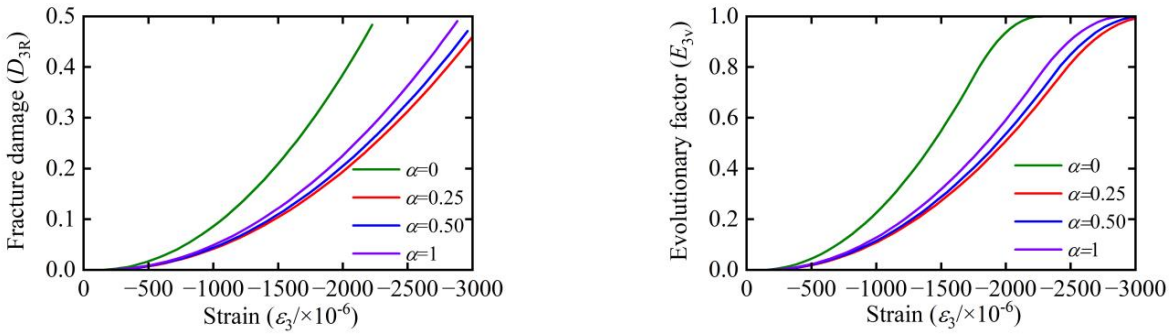


Figure 20. Mesoscopic parameters for different stress ratios: (**a**) D_{3R} evolution curve; (**b**) E_{3v} evolution curve.

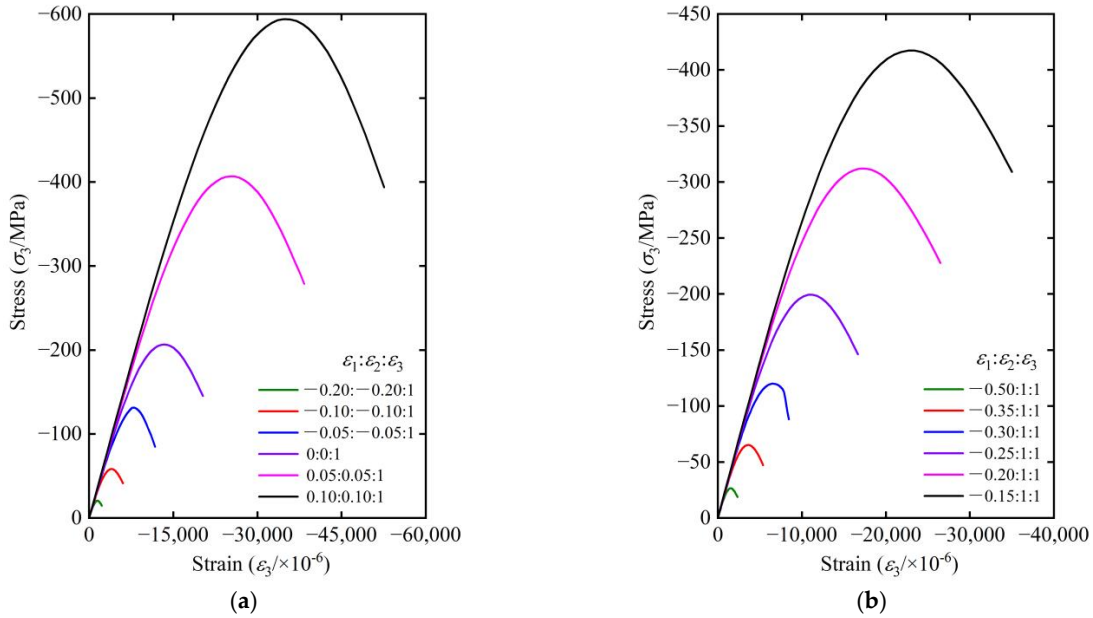


Figure 21. Curves in triaxial compression: (**a**) $\varepsilon_1 = \varepsilon_2 > \varepsilon_3$; (**b**) $\varepsilon_1 > \varepsilon_2 = \varepsilon_3$.

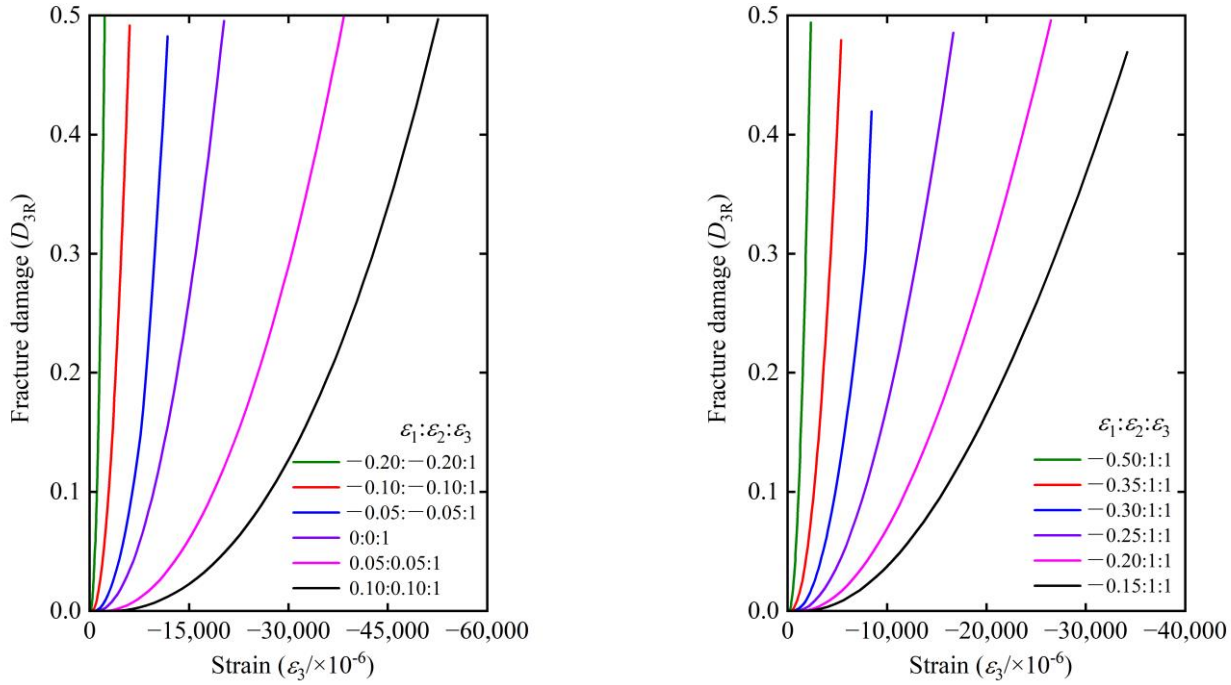


Figure 22. Evolution curves of D_{3R} in triaxial compression: (**a**) $\varepsilon_1 = \varepsilon_2 > \varepsilon_3$; (**b**) $\varepsilon_1 > \varepsilon_2 = \varepsilon_3$.

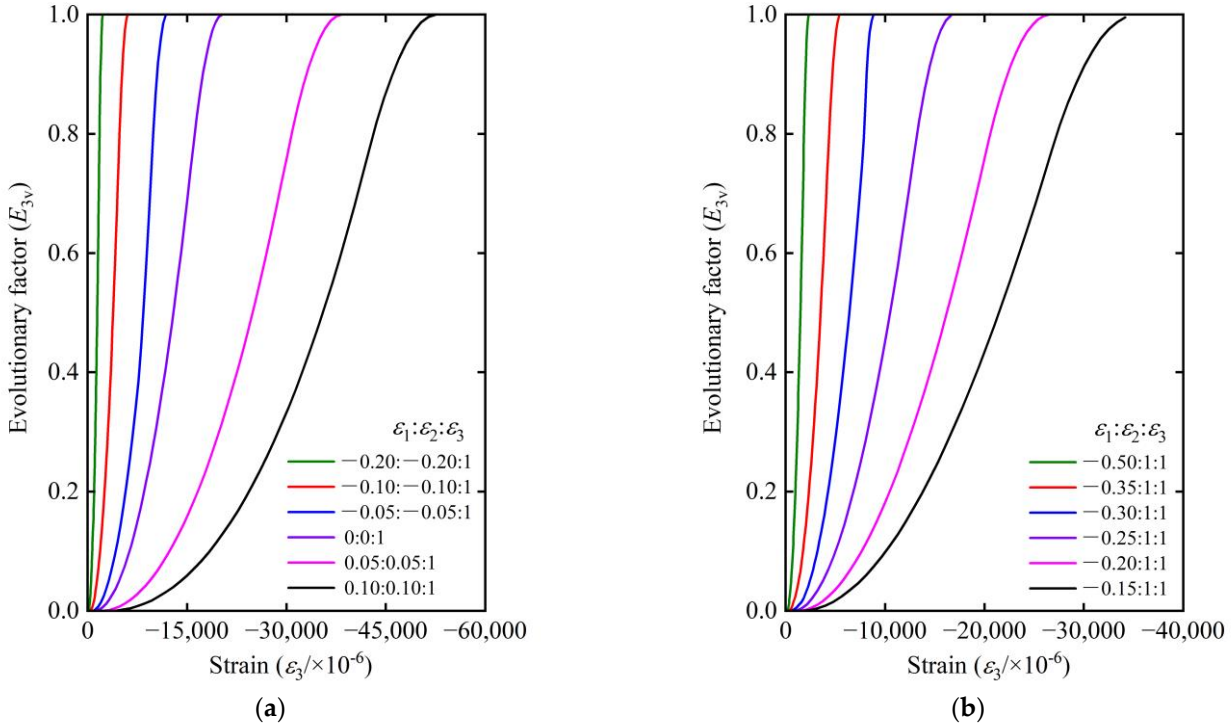


Figure 23. Evolution curves of E_{3v} in triaxial compression: (**a**) $\varepsilon_1 = \varepsilon_2 > \varepsilon_3$; (**b**) $\varepsilon_1 > \varepsilon_2 = \varepsilon_3$.

6. Discussion

The numerical simulation method proposed in this paper can effectively simulate the uniaxial, biaxial and triaxial stress characteristics of concrete.

D_R is related to the microcrack density and reflects the microcrack sprouting and expansion process. In Figure 16, under the same strain, axial compression has a lower degree of optimization and adjustment of the microstructural force skeleton than axial

tension, with a relative lag in the critical state and a higher deformation capacity. E_v is related to yield damage and reflects the degree of optimized adjustment of the concrete microstructure stress skeleton. In the uniform damage stage, E_v varies from 0 to 1 and plays a decisive role in the whole process. In Figure 17, the critical state is reached when $E_v = 1$, which means that the effective stress skeleton of the microstructure is adjusted to the optimum, the potential bearing capacity of the material is played to the limit, and enters the damage stage characterized by damage localization. Under the same strain, the degree of optimization and adjustment of microstructure effective stress skeleton for axial compression is lower than that for axial tension.

As the main part of the mesoscopic damage cumulative evolution, the uniform damage part of the nominal stress–strain curve consists of an ascending section and a partially descending section. In this section, the nominal stress first increases and then decreases; the effective stress increases monotonically, with the maximum value occurring in the critical state, after which the concrete enters the localized damage stage. In Figure 19, the biaxial relative strength envelope conforms to conventional test characteristics, which also indicates the rationality of the numerical analysis results. In Figure 20, for the biaxial compression-compression state with stress ratio α varying from 0.25 to 1, under the same strain, the larger the stress ratio, the larger the value of D_{3R}, which indicates that the density of microcracks is greater. Meanwhile, the value of E_{3v} is also increased by the increase of the stress ratio, which indicates that the critical state of the concrete is relatively forward when the stress ratio is larger, resulting in a reduction of its deformation capacity. The characteristics of the D_{3R} and E_{3v} curves for different stress ratios correspond to the nominal stress–strain curves.

From the simulation results, it can be seen that the triaxial stress state is complex. For the mode $\varepsilon_1 = \varepsilon_2 > \varepsilon_3$, the peak stress and peak strain of σ_3-ε_3 curve increase as the strain in the other two directions change from tensile strain to compressive strain, and the related D_{3R} and E_{3v} curves show regular changes. For the mode $\varepsilon_1 > \varepsilon_2 = \varepsilon_3$, the peak stress and peak strain of σ_3-ε_3 curve increase as the tensile strain ε_1 decrease, and the related D_{3R} and E_{3v} curves also show regular changes. Therefore, it can be concluded that the numerical simulation method proposed in this study is able to effectively calculate the mechanical properties of fully-graded concrete under a triaxial stress state.

7. Conclusions

This paper studies the method of numerical implementation of SDM by proposing a numerical simulation model through the FORTRAN subroutine. The reasonableness of the proposed model was verified through the uniaxial and biaxial tests. The main findings and conclusions are summarized as follows:

1. The axial tensile and compression tests of fully-graded concrete are the basis for establishing SDM. The determination of ε_a, ε_h, ε_b and H parameters is significant for establishing the constitutive relationship of fully-graded concrete. The ABC method is able to converge to the optimal parameters very quickly, and the nominal stress–strain curves predicted by the model are in good agreement with the experimental curves.
2. The numerical simulation model of SDM was proposed through FORTRAN programming. In the calculation process, the impact of damage is reflected by reducing stiffness. The whole process is to embed the FORTRAN program into the finite element software to analyze the damage evolution characteristics of the structure.
3. Under the same strain, the degree of optimization and adjustment of microstructure effective stress skeleton for axial compression is lower than that for axial tension. For the biaxial compression-compression state with stress ratio α varying from 0.25 to 1, under the same strain, the larger the stress ratio, the density of microcracks is greater; meanwhile, the critical state of the concrete is relatively forward when the stress ratio is larger, resulting in a reduction of its deformation capacity. The triaxial stress state is complex, and the stress characteristics are different under different strain ratios.

The numerical simulation method proposed in this paper is able to apply the SDM of fully-graded concrete to finite element analysis, laying the foundation for refined finite element analysis of hydraulic structures, mesoscopic damage mechanism study and structure design optimization. According to actual engineering requirements, the numerical simulation of SDM considering freeze–thaw and dynamic strain rates will be researched in the near future to further reveal the durability and seismic performance of concrete structures.

Author Contributions: Conceptualization, C.Y., C.L. and W.B.; methodology, W.B.; software, C.Y.; validation, C.Y., H.H. and Y.X.; formal analysis, C.Y. and Y.X.; investigation, H.H.; resources, C.L. and H.H.; data curation, C.Y. and Y.X.; writing-original draft preparation, C.Y.; writing—review and editing, W.B. and Y.X.; visualization, C.Y. and C.L.; supervision, W.B.; project administration, Y.X.; funding acquisition, C.Y. All authors have read and agreed to the published version of the manuscript.

Funding: This research was funded by the Open Research Fund of Key Laboratory of Construction and Safety of Water Engineering of the Ministry of Water Resources, China Institute of Water Resources and Hydropower Research, Grant No. 202110; IWHR Research & Development Support Program (No. SM0145B042021); National Natural Science Foundation of China (No. 51679092, No. 52179132); Henan Natural Science Fund for Distinguished Young Scholars (No. 232300421016) and Henan Provincial Key Young Teacher Training Program (No. 2021GGJS074).

Data Availability Statement: Data underlying the results presented in this paper are not publicly available at this time but may be obtained from the authors upon reasonable request.

Conflicts of Interest: The authors declare no conflict of interest.

Nomenclature

Symbol	Meaning
$q(\varepsilon_1)$	Probability density function of mesoscopic fracture for axial tension
$p(\varepsilon_1)$	Probability density function of mesoscopic yield damage for axial tension
D_{1R}	Damage variable related to mesoscopic fracture for axial tension
ε_{at}	Initial damage strain for axial tension
ε_{ht}	Strain corresponding to the peak value of $p(\varepsilon_1)$ for axial tension
ε_{bt}	Maximum yield damage strain for axial tension
ε_{1cr}	Critical state strain for axial tension
ε_3^+	Equivalent transfer tensile damage strain for axial compression
ν	Poisson ratio
$q(\varepsilon_3^+)$	Probability density function of mesoscopic fracture for axial compression
$p(\varepsilon_3^+)$	Probability density function of mesoscopic yield damage for axial compression
ε_{ac}	Initial damage strain for axial compression
ε_{hc}	Strain corresponding to the peak value of $p(\varepsilon_3^+)$ for axial compression
ε_{bc}	Maximum yield damage strain for axial compression
ε_{3cr}	Critical state strain for axial compression
D_{3R}	Damage variable related to mesoscopic fracture for axial compression
σ	Nominal stress
σ_E	Effective stress
ε	Strain
E_0	Initial elastic modulus
D_R	Damage variable related to mesoscopic fracture damage
D_y	Damage variable related to yield damage
E_v	Reinforcement factor related to microscopic yield damage
H	Fracture damage value for the critical state
ε_i, ε_j, ε_k	Principal directional strain
ε_{ii}, ε_{ij}, ε_{ik}	Strain components generated by the elastic stresses in the i, j and k directions in the i direction
ε_i^+	Tensile damage strain corresponding to the i direction when subjected to tension in i direction ($\varepsilon_{ii} \geq 0$)
ε_i^*	Equivalent tensile strain in the i direction due to the Poisson effect when the j and k directions are pressurized

ε_i^-	Equivalent transfer tensile strain in the i direction when the i direction is pressurized ($\varepsilon_{ii} < 0$)
k_1	Coefficient of influence of the strain component associated with the tension damage
k_2, k_3	Coefficients of influence of the strain component related to the compression damage
ε_i^-	Function of the equivalent tensile strain ε_j^*, ε_k^* induced by the Poisson effect in the j and k directions
F	Objective function
N	Number of experimental data
x_{tn}	The n-th experimental data
x_{en}	The n-th predicted value
f	Fitness function
t	Positive integer
x_{tr}	The t-th solution in the space of random parameter variations of X_r
$x_{\min,r}$	The lower bounds of the range of values of X_r
$x_{\max,r}$	The upper bounds of the range of values of X_r
x'_m	The domain parameters obtained from the m-th parameter neighborhood search performed based on x_{tr}
s	Positive integer
φ_{tr}	A random number in the range $[-1, 1]$
p	Selection probability
z	The number in the corresponding range f

References

1. Guo, J.; Lin, W.; Qin, X.; Xu, Y.; Dong, K. Mesoscopic study on fracture behavior of fully graded concrete under uniaxial tension by using the phase-field method. *Eng. Fract. Mech.* **2022**, *272*, 108678. [CrossRef]
2. Wang, H.; Wang, L.; Song, Y.; Wang, J. Influence of free water on dynamic behavior of dam concrete under biaxial compression. *Constr. Build. Mater.* **2016**, *112*, 222–231. [CrossRef]
3. Shi, L.; Wang, L.; Song, Y.; Shen, L. Dynamic multiaxial strength and failure criterion of dam concrete. *Constr. Build. Mater.* **2014**, *66*, 181–191. [CrossRef]
4. Shi, L.; Wang, L.; Song, Y.; Shen, L. Dynamic properties of large aggregate concrete under triaxial loading. *Mag. Concr. Res.* **2015**, *67*, 282–293. [CrossRef]
5. Bai, W.; Zhang, S.; Guan, J.; Chen, J. Orthotropic statistical damage constitutive model for concrete. *Shuili Xuebao* **2014**, *45*, 607–618. (In Chinese)
6. Li, J.; Ren, X. Stochastic damage model for concrete based on energy equivalent strain. *Int. J. Solids Struct.* **2009**, *46*, 2407–2419. [CrossRef]
7. Yang, G.D.; Fan, Y.; Wang, G.H.; Cui, X.Z.; Leng, Z.D.; Lu, W.B. Blast resistance of air-backed RC slab against underwater contact explosion. *Def. Technol.* **2022**, in press. [CrossRef]
8. Yang, G.; Fan, Y.; Wang, G.; Cui, X.; Li, Q.; Leng, Z.; Deng, K. Mitigation effects of air-backed RC slabs retrofitted with CFRP subjected to underwater contact explosions. *Ocean Eng.* **2023**, *267*, 113261. [CrossRef]
9. Yang, G.; Fan, Y.; Wang, G.; Cui, X.; Li, Q.; Leng, Z. Experimental and numerical investigation on dynamic behavior of RC orifice targets subjected to underwater explosions. *Eng. Struct.* **2023**, *279*, 115541. [CrossRef]
10. Yang, G.; Wang, G.; Fan, Y.; Deng, K.; Lu, W.; Zhao, J. Dynamic response and performance of submarine tunnel subjected to surface explosions. *Mar. Struct.* **2021**, *80*, 103091. [CrossRef]
11. Yang, G.; Fan, Y.; Wang, G.; Gao, Q.; Deng, K.; Wang, F. Numerical study on dynamic response of submerged tunnel subjected to underwater explosion. *Soil Dyn. Earthq. Eng.* **2022**, *156*, 107216. [CrossRef]
12. Evans, R.H.; Marathe, M.S. Microcracking and stress-strain curves for concrete in tension. *Matériaux Et Constr.* **1968**, *1*, 61–64. [CrossRef]
13. Du, C.; Chen, X.; Yang, Y.; Chen, Y.; Jiang, S. Experimental study on the complete tensile stress-deformation curve of fully graded concrete. *Exp. Tech.* **2018**, *42*, 491–497. [CrossRef]
14. Zhang, Y.H.; Hu, X.; Yang, C.; Li, C.L.; Zhu, H.; Jiao, J. Dynamic axial tension test on the fully-graded concrete. *Shuili Xuebao* **2014**, *45*, 720–727. (In Chinese)
15. Wu, J.Y.; Li, J.; Faria, R. An energy release rate-based plastic-damage model for concrete. *Int. J. Solids Struct.* **2006**, *43*, 583–612. [CrossRef]
16. Krajcinovic, D. Selection of damage parameter–Art or science? *Mech. Mater.* **1998**, *28*, 165–179. [CrossRef]
17. Hillerborg, A.; Modéer, M.; Petersson, P.E. Analysis of crack formation and crack growth in concrete by means of fracture mechanics and finite elements. *Cem. Concr. Res.* **1976**, *6*, 773–781. [CrossRef]
18. Bažant, Z.P.; Oh, B.H. Crack band theory for fracture of concrete. *Matériaux Et Constr.* **1983**, *16*, 155–177. [CrossRef]
19. Du, X.; Si, Z.; Li, Y.; Huang, L.; Si, Z.; Wen, L. Dynamic compressive behavior of freeze–thaw damaged roller-compacted concrete and establishment of constitutive model. *Constr. Build. Mater.* **2023**, *365*, 130095. [CrossRef]

20. Gou, Y.J.; Zhang, L.H.; Zhang, H.P.; Wei, C.; Yang, H.; Zhai, S.T.; Liu, L.B. Investigation of freeze-thaw mechanism for crumb rubber concrete by the online strain sensor. *Measurement* **2021**, *174*, 109080. [CrossRef]
21. Liu, M.; Liu, D.; Qiao, P.; Sun, L. Characterization of microstructural damage evolution of freeze-thawed shotcrete by an integrative micro-CT and nanoindentation statistical approach. *Cem. Concr. Compos.* **2021**, *117*, 103909. [CrossRef]
22. Suzuki, T.; Nishimura, S.; Shimamoto, Y.; Shiotani, T.; Ohtsu, M. Damage estimation of concrete canal due to freeze and thawed effects by acoustic emission and X-ray CT methods. *Constr. Build. Mater.* **2020**, *245*, 118343. [CrossRef]
23. Li, S.; Chen, X.; Zhang, J. Acoustic emission characteristics in deterioration behavior of dam concrete under post-peak cyclic test. *Constr. Build. Mater.* **2021**, *292*, 123324. [CrossRef]
24. Bažant, Z.P.; Tabbara, M.R.; Kazemi, M.T.; Pijaudier-Cabot, G. Random particle model for fracture of aggregate or fiber composites. *J. Eng. Mech.* **1990**, *116*, 1686–1705. [CrossRef]
25. Schlangen, E.; Van Mier, J.G.M. Simple lattice model for numerical simulation of fracture of concrete materials and structures. *Mater. Struct.* **1992**, *25*, 534–542. [CrossRef]
26. Xu, W.; Han, Z.; Tao, L.; Ding, Q.; Ma, H. Random non-convex particle model for the fraction of interfacial transition zones (ITZs) in fully-graded concrete. *Powder Technol.* **2018**, *323*, 301–309. [CrossRef]
27. Ma, H.; Xu, W.; Li, Y. Random aggregate model for mesoscopic structures and mechanical analysis of fully-graded concrete. *Comput. Struct.* **2016**, *177*, 103–113. [CrossRef]
28. Qin, X.; Gu, C.; Shao, C.; Fu, X.; Vallejo, L.; Chen, Y. Numerical analysis of fracturing behavior in fully-graded concrete with oversized aggregates from mesoscopic perspective. *Constr. Build. Mater.* **2020**, *253*, 119184. [CrossRef]
29. Xu, L.; Jiang, L.; Huang, Y.F.; Ren, Q.W. An efficient approach for mesoscale fracture modeling of fully-graded hydraulic concrete. *Water Sci. Eng.* **2022**, *15*, 337–347. [CrossRef]
30. Xu, L.; Jiang, L.; Shen, L.; Dong, Y.; Ren, Q. 3D mesostructure generation of fully-graded concrete based on hierarchical point cloud and aggregate coarsening. *Constr. Build. Mater.* **2022**, *350*, 128790. [CrossRef]
31. Wang, G.; Wang, Y.; Lu, W.; Yu, M.; Wang, C. Deterministic 3D seismic damage analysis of Guandi concrete gravity dam: A case study. *Eng. Struct.* **2017**, *148*, 263–276. [CrossRef]
32. Wang, G.; Wang, Y.; Lu, W.; Zhou, C.; Chen, M.; Yan, P. XFEM based seismic potential failure mode analysis of concrete gravity dam–water–foundation systems through incremental dynamic analysis. *Eng. Struct.* **2015**, *98*, 81–94. [CrossRef]
33. Chen, D.H.; Yang, Z.H.; Wang, M.; Xie, J.H. Seismic performance and failure modes of the Jin'anqiao concrete gravity dam based on incremental dynamic analysis. *Eng. Fail. Anal.* **2019**, *100*, 227–244. [CrossRef]
34. Krajcinovic, D.; Silva, M.A.G. Statistical aspects of the continuous damage theory. *Int. J. Solids Struct.* **1982**, *18*, 551–562. [CrossRef]
35. Breysse, D. Probabilistic formulation of damage-evolution law of cementitious composites. *J. Eng. Mech.* **1990**, *116*, 1489–1510. [CrossRef]
36. Kandarpa, S.; Kirkner, D.J.; Spencer Jr, B.F. Stochastic damage model for brittle materials subjected to monotonic loading. *J. Eng. Mech.* **1996**, *122*, 788–795. [CrossRef]
37. Bai, W.; Shen, J.; Guan, J.; Wang, J.; Yuan, C. Study on compressive mechanical properties of recycled aggregate concrete with silica fume at different strain rates. *Mater. Today Commun.* **2022**, *31*, 103444. [CrossRef]
38. Bai, W.; Song, Z.; Yuan, C.; Guan, J.; Xie, C.; Huang, H.; Ma, Y. Study on mechanical properties and damage mechanism of recycled concrete containing silica fume in freeze–thaw environment. *Constr. Build. Mater.* **2023**, *375*, 130872. [CrossRef]
39. Bai, W.; Lu, X.; Guan, J.; Huang, S.; Yuan, C.; Xu, C. Stress–strain behavior of FRC in uniaxial tension based on mesoscopic damage model. *Crystals* **2021**, *11*, 689. [CrossRef]
40. Bai, W.; Lu, X.; Guan, J.; Yuan, C. Experimental study on uniaxial compression mechanical properties of recycled concrete with silica fume considering the effect of curing age. *Constr. Build. Mater.* **2022**, *350*, 128758. [CrossRef]
41. Bai, W.; Li, W.; Guan, J.; Wang, J.; Yuan, C. Research on the mechanical properties of recycled aggregate concrete under uniaxial compression based on the statistical damage model. *Materials* **2020**, *13*, 3765. [CrossRef] [PubMed]
42. Bai, W.; Wang, W.; Guan, J.; Wang, J.; Yuan, C. Compressive stress-strain relationships of concrete exposed to elevated temperatures based on mesoscopic damage method. *Int. J. Damage Mech.* **2022**, *31*, 1420–1447. [CrossRef]
43. *SL/T 352-2020*; Test Code for Hydraulic Concrete. Ministry of Water Resources of the People's Republic of China: Beijing, China, 2020. (In Chinese)

Disclaimer/Publisher's Note: The statements, opinions and data contained in all publications are solely those of the individual author(s) and contributor(s) and not of MDPI and/or the editor(s). MDPI and/or the editor(s) disclaim responsibility for any injury to people or property resulting from any ideas, methods, instructions or products referred to in the content.